J. Wind Eng. Ind. Aerodyn. 134 (2014) 44–55

Contents lists available at ScienceDirect

Journal of Wind Engineering and Industrial Aerodynamics

journal homepage: www.elsevier.com/locate/jweia

Experimental fragility curves for aluminum storm panels subject to windborne debris impact

T.C. Alphonso, M. Barbato *

Department of Civil and Environmental Engineering, Louisiana State University, Patrick F. Taylor Hall, Baton Rouge, LA 70803, USA

ARTICLE INFO

Article history:
Received 17 April 2014
Received in revised form
13 August 2014
Accepted 16 August 2014

Keywords:
Hurricane hazard
Performance-based design
Windborne debris
Fragility curves
Storm panels

ABSTRACT

This paper presents the derivation of experimental fragility curves for windborne debris (WBD) impact risk assessment of aluminum storm panels within a recently developed performance-based hurricane engineering (PBHE) framework. By using a pneumatic wind cannon, rod-type WBDs were fired at aluminum storm panels to evaluate the effects of WBD impact hazard. The experimental data from testing were used to derive the probability of failure relative to specific damage measures (DMs) versus its corresponding interaction parameter (IP). These experimentally derived probabilities were also compared with finite element-based results that were available in the literature.

It was found that the impact kinetic energy of rod-type missiles is a sufficient IP for aluminum storm panels subjected to WBD impact, the probability of penetration of aluminum storm panels is strongly dependent on the details of the panels' installation, and the numerical results available in the literature regarding the fragility curves of storm panels are qualitatively representative of the behavior of aluminum storm panels subject to WBD impact. It is noteworthy that accurate fragility curves are essential in the development of a general probabilistic performance-based engineering framework for mitigation of WBD impact hazard.

1. Introduction

Extreme weather events such as hurricanes and tornados have repeatedly caused severe damage to structural and infrastructural systems in the United States of America (NSB, 2007; Pielke et al., 2008) and worldwide (Kentang, 2000; Stewart, 2003). Even tropical storms have led to significant structural damage, sometimes even causing the loss of life. Thus, it is critical for engineers to design structures that can safely withstand the loading conditions accompanying these natural events.

Over the past decade, significant advances in risk assessment and mitigation for structures subjected to hurricane hazards have been achieved (Li and Ellingwood, 2006; Holmes, 2008, 2010). Structural reliability analysis and the development of probabilistic performance-based engineering (PBE) techniques have been two key elements to the growth and advances in this research and practice field. Modern structural reliability analysis techniques rigorously account for uncertainties in engineering design and can be used to develop more rational design codes (Nowak, 1999; Kwon et al., 2010). Probabilistic performance-based methods have been extensively developed in the field of earthquake engineering (Cornell and Krawinkler, 2000; Porter, 2003) and have already been used to develop modern seismic design codes (ATC, 1997, 2005). Similar methodologies, which are based on a PBE approach, have been advancing also in other civil engineering subfields including wind engineering, fire engineering, and blast engineering (Hamburger and Whittaker, 2003; Augusti and Ciampoli, 2006; Li and Ellingwood, 2006; Rini and Lamont, 2008; Ciampoli et al., 2011). Recently, a performance-based hurricane engineering (PBHE) framework has been proposed to extend PBE to the analysis and design of structures subject to hurricane hazard (Barbato et al., 2013).

A critical feature of probabilistic PBE methods is the explicit consideration of all pertinent uncertainties that can affect the performance of a structure. Probabilistic PBE methodologies require the development of several analytical and numerical tools to propagate these uncertainties from the environmental actions to the performance of structural systems. Amongst these tools, fragility curves are probably the most significant (Gardoni et al., 2002; Lupoi et al., 2006). They are the cumulative distribution functions (CDFs) of the structural capacity relative to a specific limit-state, usually corresponding to a physical damage state for the structural system under consideration (Mackie and Stojadinovic, 2004).

In hurricane engineering, only a few studies have focused on fragility analysis (ATC, 2005; Gurley et al., 2005; Li and Ellingwood, 2006). Thus, fragility curves for many structural and non-structural

* Corresponding author.
E-mail addresses: talphonso@chevron.com (T.C. Alphonso), mbarbato@lsu.edu (M. Barbato).

http://dx.doi.org/10.1016/j.jweia.2014.08.010
0167-6105/

components of buildings subject to hurricane actions are still needed in order to facilitate the use of the PBHE framework. In particular, fragility curves for the non-structural components constituting the building envelope (e.g., non-load-bearing walls, windows, doors, roofing, and protection elements) are crucial to evaluate the performance of buildings located in hurricane prone regions, since buildings are exposed to a significantly higher damage risk when their building envelopes are compromised (Li and Ellingwood, 2006; Lopez et al., 2011). A typical issue for building envelope components is the loading due to windborne debris (WBD) impact. Numerous studies investigated WBD hazard for residential buildings. Earlier studies focused on a deterministic treatment of WBD impact (Minor et al., 1978; Tachikawa, 1983, 1988; McDonald, 1990). More recently, the attention of the engineering community shifted to risk analysis (Twisdale et al., 1996; Holmes, 2008, 2010; Lin and Vanmarcke, 2010; Lin et al., 2010) and damage analysis (NAHB, 2002; Willis et al., 2002; Masters et al., 2010; Fernandez et al., 2010), and led to improved standardized tests for WBD impact resistance (ASTM, 2005a, 2005b) and to probability-based damage models for building envelope components subject to WBD impact hazard (Pinelli et al., 2004; Gurley et al., 2005; ATC, 2005). However, only scarce information is available regarding the fragility of building envelope components with ductile behavior. Borges et al. (2009) studied the finite element modeling of aluminum and galvanized steel storm panels subject to wooden windborne debris impact. Fernandez et al. (2010) investigated the experimental performance of aluminum and steel storm shutters subject to the impact of wooden missiles and concrete roof tiles under similar conditions to those enforced in the tests used for product certification. Laboy et al. (2013) examined the likelihood of the puncture of metal shutters by roof tile debris based on hurricane intensity.

This research focuses on the evaluation of experimental fragility curves that represent the damage states for aluminum storm panels subjected to WBD impact loading. Aluminum storm panels are building envelope components with ductile behavior. In this paper, a brief overview of the PBHE framework is presented, followed by the description of the experimental apparatus used to fire lumber missiles at the aluminum storm panels and the research results in terms of experimental fragility curves. These experimental fragility curves are compared with numerical results available in the literature and based on finite element simulation of the impact between wooden missiles and aluminum panels. Additional considerations are provided on the applicability and scope of this research. Finally, relevant conclusions are drawn.

2. Performance-based hurricane engineering (PBHE) framework

Fragility curves for structural and non-structural components are useful tools in several wind engineering applications. In particular, they are crucial ingredients of the performance-based hurricane engineering (PBHE) framework that was recently proposed in Barbato et al. (2013). This framework accounts for the effects on structural performance of the different hazard sources (i.e., strong winds, windborne debris, flooding, and rain) that are related to hurricane landfalls. This PBHE framework is based on the total probability theorem (Ang and Tang, 1975) and disaggregates the performance assessment procedure for structures subject to hurricane hazard into elementary phases, which are carried out in sequence. An important feature of the PBHE procedure is the qualitative independence of each phase from the others (i.e., the choice of the parameters that are characteristic for a given phase is independent from the parameters adopted in the previous phases). PBHE is a multi-hazard approach that considers the interaction among different hazard sources, whereas other established PBE frameworks focus on a single hazard.

The risk assessment procedure is disaggregated into the following six separate tasks, each providing the probabilistic description of different sets of variables (which are indicated in parentheses for each task): (1) hazard analysis (intensity measures: IM), (2) structural characterization (structural parameters: SP), (3) interaction analysis (interaction parameters: IP), (4) structural analysis (engineering demand parameters: EDP), (5) damage analysis (damage measures: DM), and (6) loss analysis (decision variable: DV). Fragility curves are obtained from the convolution of the results derived from damage analysis and structural analysis. An important consequence of the inclusion of the interaction analysis phase in PBHE is that fragility curves must be expressed as functions of IP rather than of IM, as customarily done in other PBE approaches. The determination of an appropriate scalar or vector IP for a specific response quantity of a specific structure subjected to a specific hazard is an integral part of the PBHE methodology and follows the same criteria of sufficiency and efficiency used, e.g., in Performance-Based Earthquake Engineering to determine appropriate IM (Baker and Cornell, 2005, 2008; Vamvatsikos and Cornell, 2005; Luco and Cornell, 2007).

3. Experimental setup and test specimens

This section describes the experimental setup used to determine experimental fragility curves, as well as the properties and configurations of the aluminum storm panels and wooden missiles used in the tests. The fragility curves presented in this paper are based on experimental results obtained from firing 2×4 lumber missiles (with actual finished dimensions equal to $1\text{-}1/2''\times3\text{-}1/2''=38$ mm $\times$ 89 mm) at aluminum storm panels using a pneumatic wind cannon. The experimental campaign was performed using the Louisiana State University Wind Cannon (LSUWC), which is located at the LSU Blowout Prevention Facility in Baton Rouge, LA. The experimental equipment consists of: (1) a steel pneumatic cannon (i.e., the LSUWC), (2) a velocity measurement system, (3) a support target frame, and (4) a deflection measurement system.

3.1. LSU wind cannon (LSUWC)

The LSUWC is a pneumatically actuated steel cannon with computer control that fires projectiles (e.g., 2×4 lumber missiles and small steel balls), which simulate WBD caused by hurricane force winds. The LSUWC main components are shown in Fig. 1. They include: (1) a steel barrel of length equal to 15′ (4.57 m) with a 6″ (15.2 cm) nominal diameter; (2) a 30-gal (113.56 l) tank located above the barrel, which is used to hold pressurized air (with a nominal capacity of 300 psi = 2.068 MPa); (3) a pressure gage and a pressure control valve, which are used to achieve the desired air pressure within the tank; and (4) a base structure, which sustains the barrel and the tank, facilitate the transportation of the cannon, and controls its vertical and horizontal movements. A mechanical winch attached to the base structure controls the vertical movement of the cannon, while the horizontal (side-to-side) movement of the cannon is controlled by a hand-operated pulley, which is also an integral component of the base structure (Fig. 1).

The air pressure achieved within the tank provides the force needed to drive the projectile to the desired velocity. The amount of pressure contained within the tank can be instantly released by a 6″ (15.2 cm) pneumatic butterfly valve. This butterfly valve can

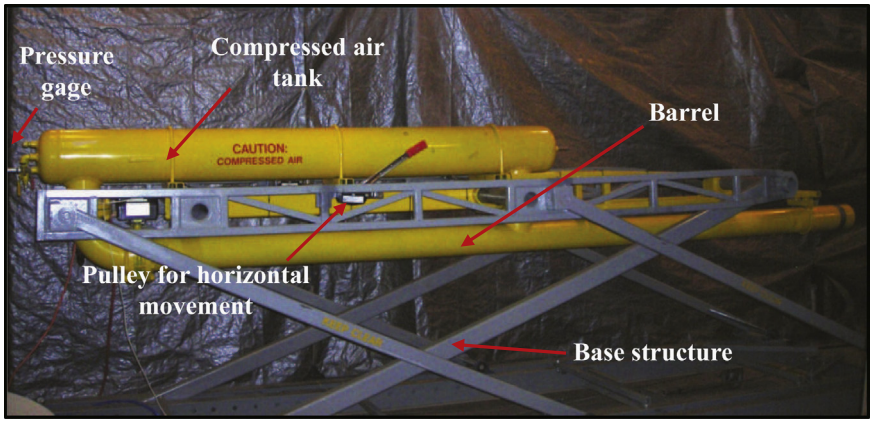

Fig. 1. Main components of the LSUWC.

be opened through a master air cylinder that is controlled by a four-way 110V AC solenoid valve. The solenoid-operating signal originates from a lockable firing box, which includes an indicator light (when lit, it indicates that the air in the tank is pressurized), a firing button, and a safety-keyed switch that stops the air flow in order to avoid accidental firing of the cannon.

3.2. Velocity measurement system

The velocity measurement system for the missile velocity consists of a shooting chronograph with a dual sensor system, which provides accurate projectile velocities that can be recorded using different units of measure. The chronograph used in this research is the Beta Master Chrony chronograph produced by the company Shooting Crony (Shooting Chrony, 2014). This chronograph exceeds the ASTM E1866 and E1996 standard specifications for hurricane WBD impact testing (ASTM, 2005a, 2005b) and has an accuracy of $\pm$ 1% of the specified speed in the velocity measurements. The device houses two light sensors that are strategically placed at an accurately measured separation distance. As a projectile breaks the first sensor's plane, the sensor transmits a signal to the circuit board, which records the time when the first sensor's plane is broken. When the projectile breaks the second sensor's plane, another signal is sent to the circuit board, which records the time at which the second sensor's plane is broken. The difference between these two times is used to calculate the velocity of the projectile, *V*. The chronograph was placed so that the first light sensor was engaged after the missile had finished accelerating.

The Beta Master Chrony chronograph has a detachable liquid-crystal display to present the recorded velocity. The unit is able to store up to 1000 readings, which can then be readily transferred to computer applications for post-processing of the data. This chronograph is equipped with two small light diffusers, which can be placed above each sensor in order to assure the best lighting conditions for each sensor. However, these diffusers are intended for use with small projectiles. For this research, a larger diffuser was built to ensure appropriate lighting conditions for accurate velocity readings, since the open distance between the two sensors and the small light diffusers was insufficient for safe firing of the 2×4 lumber missiles.

3.3. Target support frame

The testing operations for this research were performed inside a standard $8' \times 8' \times 20'$ (2.44 m $\times$ 2.44 m $\times$ 6.10 m) steel shipping container located at the LSU Blowout Prevention Facility. This container provides a self-contained protection system for operators

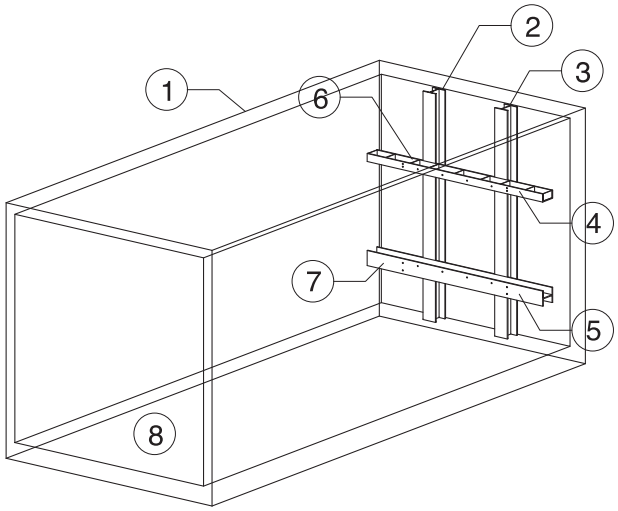

Fig. 2. REVIT model of the target support frame.

and bystanders during the testing activities, as well as a permanent storage option to protect the cannon from the outside environment when not in use. A steel target support frame is permanently attached to the rear of the testing container while still allowing for enough storage space for the cannon. The target support frame was designed to withstand the impact forces from the tests with negligible deflections. Fig. 2 shows an Autodesk REVIT Structure (Autodesk Inc., 2013) model of the target support frame. The components of the frame are: (1) shipping container (20′ standard); (2) and (3) left and right vertical supports ($W6 \times 25$ beams), respectively; (4) top horizontal support ($C6 \times 12$ channel); (5) bottom horizontal support ($W6 \times 20$ beam); (6) top welded connection; (7) bottom welded connection; and (8) container floor (2×6 wood boards). The test specimens are connected to the horizontal support beams via bolts or other elements to reproduce boundary conditions that are consistent to those used in real-world applications.

3.4. Deflection measurement system

The experimental equipment used in this research includes a measurement system for both maximum deflections and plastic deformations due to WBD impact. The maximum deflection measurements are needed to build the fragility curve of the aluminum panels corresponding to failure of the protected window, whereas the plastic deformation measurements are needed

to build the fragility curve of the aluminum panels corresponding to failure of the panel.

Plastic deformations are easily measured while the panel is still connected to the frame after impact by using the horizontal support beams as reference system, a straight beam lying vertically against the horizontal support beams, and a square ruler. The maximum deflection measurement system consists of aluminum (stiff) dryer vents positioned behind the test panel (i.e., on the opposite side from the impact). This measurement system was devised based on recommendations made by the Miami-Dade Building Code Compliance Office testing department (Miami-Dade BCCO, personal communication). Two different configurations were used in the tests: (1) a single 4″ (10.2 cm) dryer vent extended 75% pressing upon the rear of the panel for the tests in which the impact location was in the middle of the panel, and (2) multiple 2″ (5.1 cm) dryer vents extended 75% pressing upon the rear of the panel for other impact locations. In both configurations, the dryer vent is in the horizontal direction parallel to the projectile's traveling direction. Fig. 3 shows the installation and use of a dryer vent for impact deflection measurements, as well as a graphical representation of the measured plastic deformation and maximum deflection.

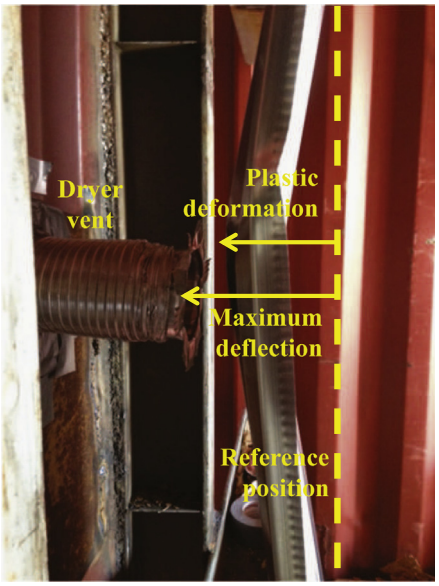

Fig. 3. Deflection measurement system.

3.5. *Experimental specimens: aluminum storm panels and wooden missiles*

This research focuses on corrugated aluminum storm panels, which are commonly used in hurricane prone regions to protect brittle building envelope components (Fig. 4a). These storm panels are characterized by relatively low cost, mobility, and ease of installation. The aluminum storm panels considered here have height $H=47.25$ in (120.01 cm), and width $W=14.37$ in (36.51 cm) and are made of 0.05 in (1.27 mm) gauge 3004H34 type aluminum. A typical cross-section of the panel is shown in Fig. 4b.

Three sets of 2×4 missiles were considered: 9-lb, 12-lb, and 15-lb missiles, corresponding to masses of 4.08 kg, 5.44 kg, and 6.80 kg, respectively. The 2×4 missiles used in the test followed the guidelines of the ASTM E1996 Standard (ASTM, 2005a). It is noteworthy that the 12-lb missile is not included in the ASTM E1996 specifications. The missiles were connected to a sabot before firing (Fig. 4c). The sabot consisted of a circular cut section of medium density fiberboard. These sabots were cut to measure exactly 5-5/8″ (14.3 cm) in diameter, in order to ensure that a proper thrust was available to the projectile. It is noteworthy that 2×4 wooden missiles were selected for this research because their use is required in the ASTM impact test standards (as well as in previous standards) for the large missile tests. This choice facilitates the comparison of the results presented in this study with those customarily obtained in product acceptance tests. However, it should be also noted that, in residential settings, roof shingles were found to be a dominant source of wind-borne debris when compared to the 2×4 wooden missiles used in standardized test methods (NAHB, 2002).

4. Experimental results and discussion

The experimental component of this research achieved the following results: (1) the derivation of pressure–velocity curves for the LSUWC, (2) the determination of a suitable IP for ductile building envelope components, (3) the identification of different impact typologies, (4) the statistical characterization of the EDPs

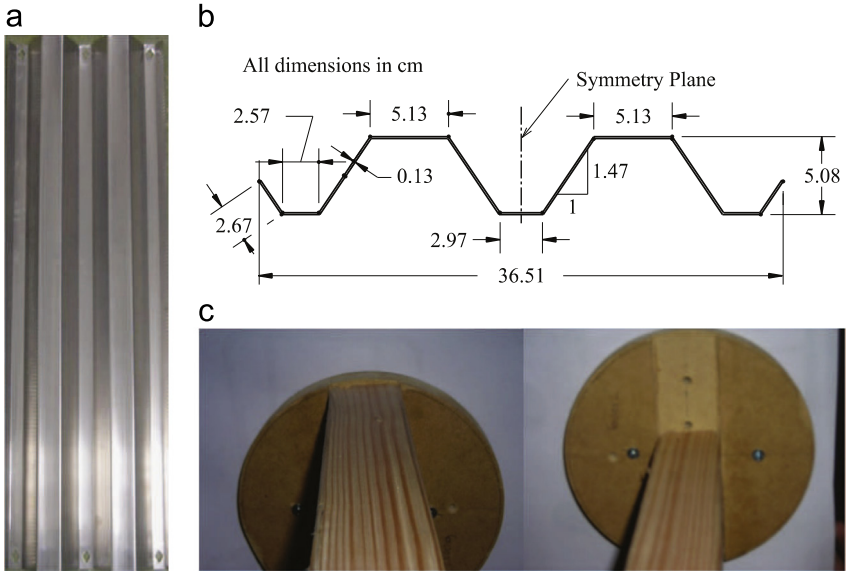

Fig. 4. Experimental specimens: (a) picture of an aluminum storm panels, (b) typical cross-section of a storm panel, and (c) sabot attachment to a 2×4 wooden missile.

for ordinary impacts, and (5) the evaluation of the effects of different boundary conditions for the aluminum panels. Each aluminum panel was used for a single impact test and then discarded.

4.1. Derivation of pressure–velocity curves for the LSUWC

The use of the LSUWC requires the derivation of different pressure–velocity curves for different projectiles. These pressure–velocity relations are used to set the pressure in the air tank and to produces the desired velocity for the projectile within a specified accuracy. Due to the large number of variables affecting the projectile's velocity (e.g., air leaking around the sabot, inclination and positioning of the missile within the barrel), as well as the significant uncertainties affecting these variables, the pressure–velocity curves were obtained experimentally for the three different types of missiles considered in this research (i.e., 9-lb, 12-lb, and 15-lb missiles).

The velocity measurement system was calibrated through a repeatability test consisting of five missiles fired at the same air pressure for each projectile type. Then, the pressure–velocity curves for the three missile types were derived by firing several missiles at a specified air pressure and by measuring the missile velocities using the velocity measurement system. This procedure was repeated for each missile type (9-lb, 12-lb, and 15-lb) with a pressure range from 5 psi (34.47 kPa) to 30 psi (206.85 kPa). The actual pressure ranges were different for the three missile types, due to safety issues that limited the upper bound of the velocity for the 9-lb missiles and accuracy issues that limited the lower bound for the velocity of the 12-lb and 15-lb missiles. At least three firings were conducted for each missile type and each pressure value, at intervals of 1 psi from 5 psi to 20 psi, and at intervals of 2 psi from 20 psi to 30 psi. Mean and standard deviations were computed for each set of data points, and analytical pressure–velocity relations were derived through least-square fitting of the mean results for each pressure value as follows:

$$V = \begin{cases} 26.145\ln(p) - 89.843, & 34.47 \le p \le 165.47 \quad (9-\text{lb}) \\ 22.708\ln(p) - 78.694, & 48.26 \le p \le 206.84 \quad (12-\text{lb}) \\ 23.137\ln(p) - 88.696, & 68.95 \le p \le 206.84 \quad (15-\text{lb}) \end{cases} \tag{1}$$

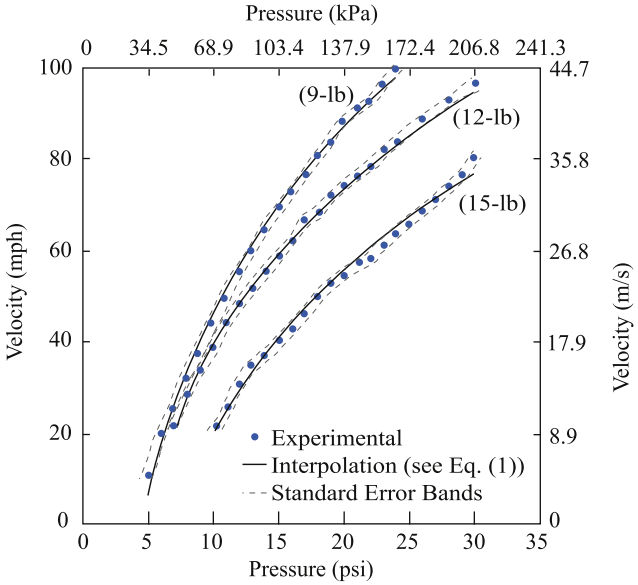

Fig. 5. Pressure–velocity curves of 2 × 4 wooden missiles for the LSUWC.

in which V denotes the missile velocity (in m/s) and p denotes the air pressure (in kPa). Eq. (1) also provides the pressure ranges within which the analytical pressure–velocity relations are valid for each missile type. Fig. 5 provides the pressure–velocity curves for the 9-lb, 12-lb, and 15-lb 2 × 4 wooden missiles.

4.2. Determination of a suitable IP

A first set of experiments was performed to determine an appropriate IP for aluminum panels. The panels were bolted at the top and bottom (i.e., on the short sides) to the horizontal beams of the support frame, in order to reproduce typical installation conditions (Fig. 6a and b). The following three potential IPs were considered: (1) missile impact velocity, V_m; (2) missile impact linear momentum, LM_m; and (3) missile impact kinetic energy, KE_m. To evaluate the sufficiency of each IP, a WBD impact test was conducted using a constant impact location corresponding to the center of the panel (Fig. 6b). The impacts occurred at various levels of the possible IPs, which were obtained by considering missiles of three different sizes (i.e., 9-lb, 12-lb, and 15-lb) and several different velocities, for a total of 62 impact tests. An IP is considered sufficient for a given EDP of interest if the EDP conditioned on IP is independent of other parameters (e.g., mass of the missile). During each impact test, the values of the following two EDPs were recorded: (1) the maximum total deflection of the storm panel during impact, Δ_{max} (which is related to the damage to the windows protected by the storm panel); and (2) the plastic deflection of the storm panel after impact, Δ_{pl} (which is related to the damage to the storm panel). The values of Δ_{max} and Δ_{pl} recorded from this testing with fixed impact point near the center of the storm panels were denoted as Δ^0_{max} and Δ^0_{pl}, respectively.

Fig. 6c–e plot the experimental EDP values versus V_m, LM_m, and KE_m, respectively. It is observed that, when the EDPs are plotted as functions of V_m and LM_m, both Δ^0_{max} and Δ^0_{pl} present a significant scatter. This scatter suggests that the EDPs are dependent on V_m and LM_m, with approximately a linear functional dependency, as well as on the weight of the missile. The results presented in Fig. 6e indicate that Δ^0_{max} and Δ^0_{pl} present a significantly smaller scatter when they are plotted as functions of KE_m, and they are practically independent of the mass of the missile. It was also experimentally observed that, for an impact kinetic energy $KE_m \ge 1.150$ kJ (denoted by a vertical dashed line in Fig. 6e), all tested storm panels failed due to penetration of the missile or failure of the connection with the support frame. For values of impact kinetic energy higher than 1.150 kJ, the experimental deflection measurements have a different physical meaning than those corresponding to lower values of the KE_m, as shown in Fig. 6e by the change in the relation between KE_m and EDPs. Fig. 7a shows a storm panel failure due to tearing near the bolts from the support frame for $KE_m = 1.175$ kJ, whereas Fig. 7b shows a panel failure from complete penetration for $KE_m = 1.500$ kJ.

Based on the results presented here, it was concluded that KE_m is the only sufficient IP, among those considered in this research, for aluminum panels. It is hypothesized here that KE_m may be a sufficient IP for building envelope components with ductile behavior in general; however, this hypothesis needs to be tested via additional experimental investigations. In addition, $KE_m = 1.150$ kJ was identified as the strength limit for the considered aluminum storm panel impacted by wooden 2 × 4 missiles.

4.3. Experimental CDFs of the EDPs and identification of impact typologies

The structural analysis phase of PBHE provides the statistical description of the EDPs conditional to the value of the identified IP

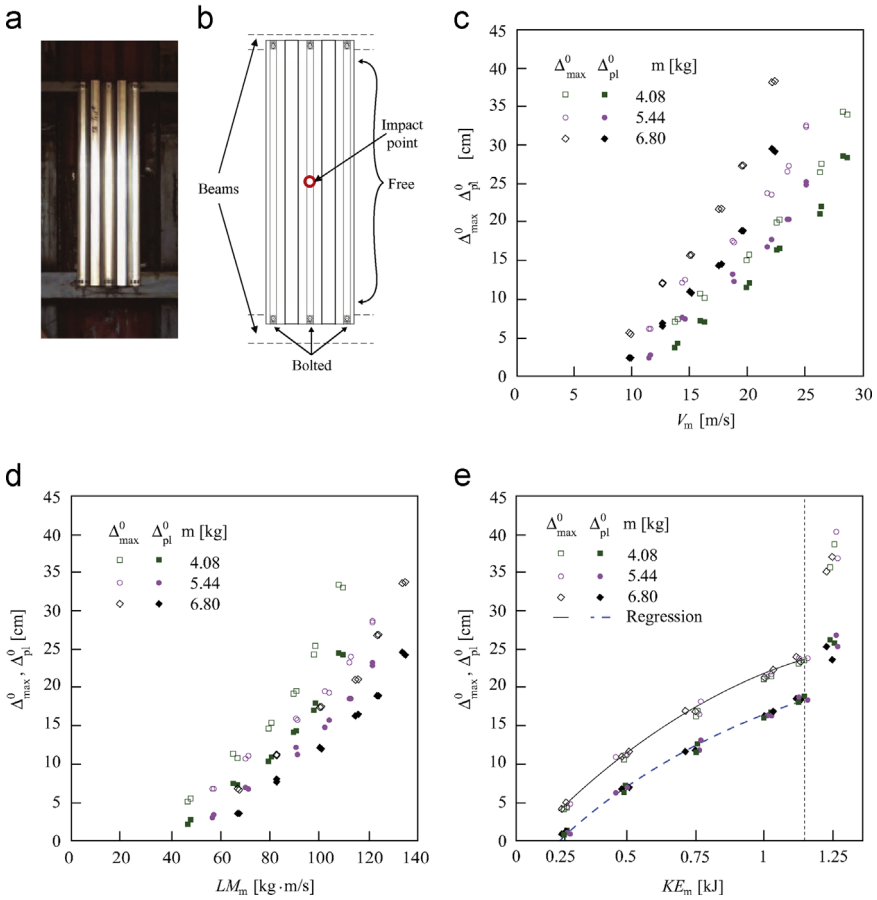

Fig. 6. Identification of a sufficient IP: (a) picture of a panel before impact, (b) drawing of boundary conditions, (c) plot of EDPs versus V_m, (d) plot of EDPs versus LM_m, and (e) plot of EDPs versus KE_m.

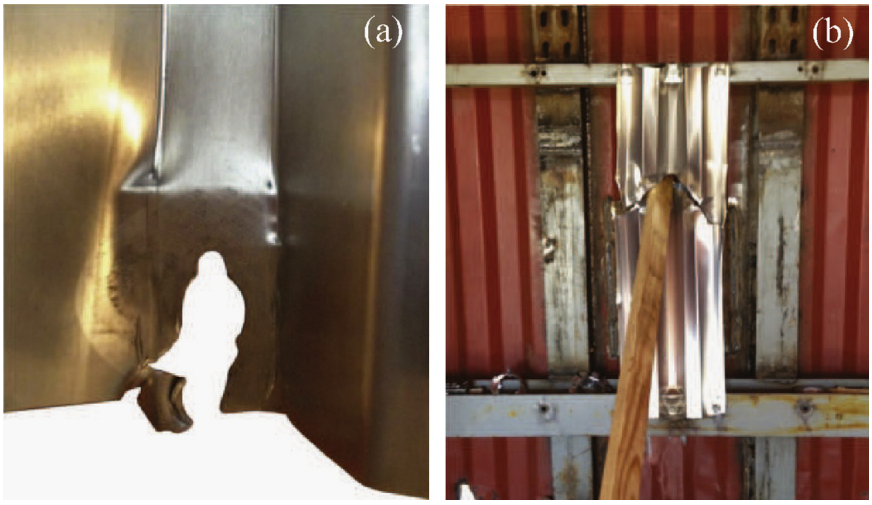

Fig. 7. Storm panels' failures: (a) tearing near the bolted connections ($KE_m = 1.175$ kJ), and (b) complete penetration ($KE_m = 1.500$ kJ).

(i.e., KE_m). A second set of tests was performed to derive the experimental relation between EDPs and KE_m for the considered storm panel corresponding to three IP levels, i.e., $KE_m = 0.250$ kJ, 0.500 kJ, and 0.750 kJ. Only one missile size was used (i.e., the 9-lb missile). The impact locations were selected randomly using a uniform distribution for both horizontal and vertical coordinates. A total of 48 impact tests were performed (i.e., 16 impacts for each level of KE_m). Due to the variability of the actual missile velocity when using the pressure–velocity curves derived for the 9-lb missile, the measured impact kinetic energy also presented a small variability (e.g., for the tests corresponding to a nominal value of $KE_m = 0.500$ kJ, the experimentally measured impact kinetic energy was contained in the range $0.488 \text{ kJ} \le KE_m \le 0.513$ kJ). This variability was neglected in the construction of the relations between EDPs and KE_m. It is noted here that this variability is very small and, thus, has a negligible effect on the results reported in the remainder of the paper. As in the previous set of experimental tests, the boundary conditions considered in this set of tests were bolted connections along the two shorter sides and free ends along the two longer sides of the storm panel (Fig. 6a). This set of tests was used to derive experimental CDFs for Δ_{max} and Δ_{pl} and to

verify that different types of impacts can be identified based on the location of the impact point, as suggested by finite element-based results available in the literature (Herbin and Barbato, 2012).

Fig. 8a and b plots the experimental CDFs for Δ_{max} and Δ_{pl}, respectively, for $KE_m = 0.250$ kJ, 0.500 kJ, and 0.750 kJ. The following three different response regions can be identified in the experimental CDFs plotted in Fig. 8: (1) a region with a concentration of very small values of Δ_{max} and Δ_{pl}, corresponding to "boundary impacts"; (2) a region with values of Δ_{max} and Δ_{pl} that are more evenly distributed, corresponding to "ordinary impacts"; and (3) a region where the missile penetrated the aluminum storm panel, corresponding to "penetrations". Using an approach commonly employed in other PBE frameworks, an infinite value of maximum and plastic deformation was associated to penetration events, and only their number was recorded experimentally and reported in Fig. 8.

A better understanding of the results reported in Fig. 8 is achieved by analyzing the WBD impact locations and the corresponding impact typologies. Fig. 9 shows the locations of the impacts and their classification into boundary impacts, ordinary impacts, and penetrations for the three levels of KE_m considered. It also identifies the regions where the three types of impacts are most likely to happen.

When the impact locations occur in the portion of the aluminum storm panel that is connected to the frame, as well as in an additional region that extends from the short side boundary connections by half of the height of the 2×4 missile (i.e., 4.445 cm), the projectiles impact the support frame. If the frame is significantly stiffer than the panel (which is the common condition for almost all residential construction), the values of Δ_{max} and Δ_{pl} are very small because they are limited by the presence of the frame (Herbin and Barbato, 2012). These boundary conditions result in a net reduction of the vulnerable area of the panel. The EDP values for these impacts typically depend on the properties of the structural component on which the storm panel is installed. The results presented in Fig. 9 also show that the impact locations corresponding to penetrations are concentrated in the portions of the aluminum storm panel that are located near the unconstrained sides. These portions can be approximately identified with two symmetric parabolic segments with base $b = 103.51$ cm and height $h = 6.35$ cm. The total sum of these two parabolic areas consists of roughly 20% of the total panel area, which is very close to the ratio between number of penetrations and total number of impact analyses obtained in this research (i.e., 2 penetrations out of 16 random impacts for $KE_m = 0.250$ kJ, with a 12.50% ratio; and 3 penetrations out of 16 random impacts for $KE_m = 0.500$ kJ and $KE_m = 0.750$ kJ, with a 18.75% ratio). Thus, the experimental results obtained in this research confirm that the probability of penetration for an aluminum storm panel is strongly dependent on the boundary conditions (i.e., on the connection details). It is noteworthy that, for $KE_m \geq 1.150$ kJ, the penetrations correspond to tearing of the panels at the bolted connections (Fig. 7a) or puncturing of the panels (Fig. 7b), similar to the failure mode observed in Laboy et al. (2013) for roof tile debris. However,

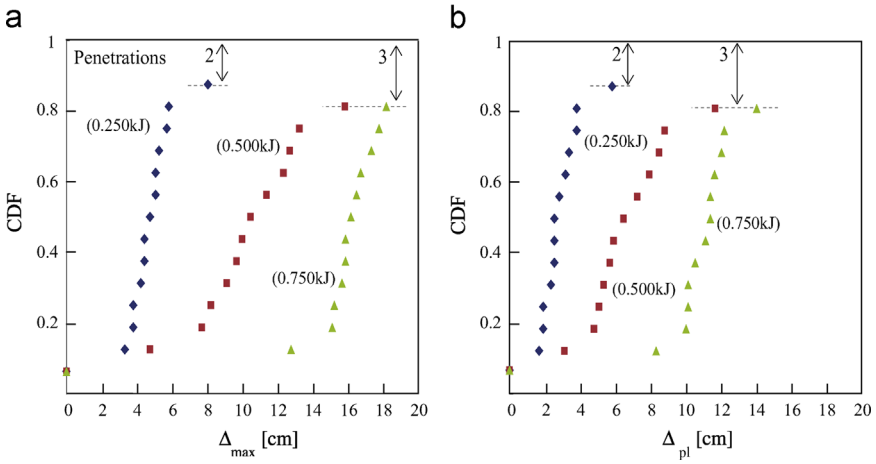

Fig. 8. Experimental CDFs for: (a) Δ_{max}, and (b) Δ_{pl}.

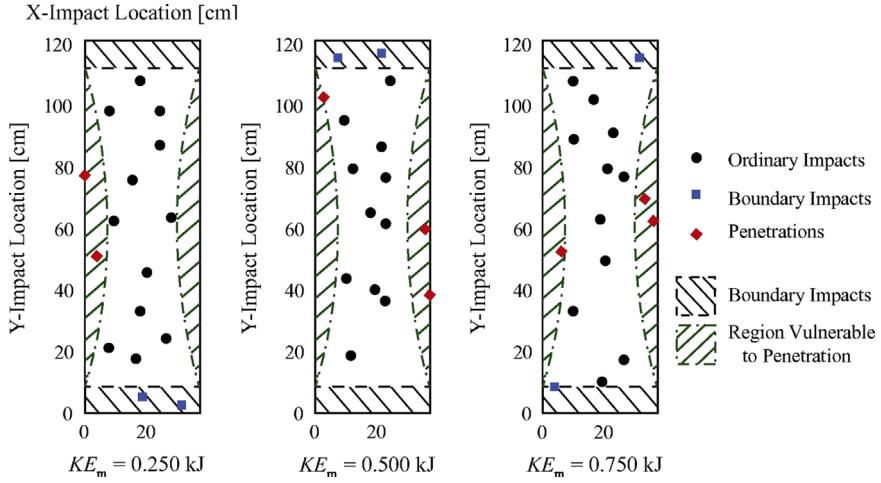

Fig. 9. Impact locations and corresponding impact types.

for $KE_m \leq 0.750$ kJ, the penetrations correspond to twisting of the panel's unsupported sides and slipping of the missiles over the panel's surface, as observed in Borges et al. (2009) and Herbin and Barbato (2012).

When an impact occurs in the portion of the panel that is not on the boundary connection or in the region vulnerable to penetration, an ordinary impact is expected, for which finite EDP values are obtained that are typically larger than those corresponding to boundary impact. For ordinary impacts, it is of interest to identify appropriate probability distributions that can be used to describe the fragility curve corresponding to the limit states of damage to the panel and to the window.

4.4. Statistical characterization of the EDPs for ordinary impacts

Experimental CDFs were obtained for the three values of KE_m considered by using only the values of the EDPs measured from ordinary impacts (i.e., not including the results that corresponded to boundary impacts and/or penetrations) and normalizing the probability of those results to one. From these values, the means and standard deviations for Δ_{max} and Δ_{pl} were computed. The normal, lognormal, and truncated normal (with lower truncations at $\Delta_{max}=0$ cm and $\Delta_{pl}=0$ cm) distributions were compared in order to find the best fit to the ordinary impacts' results. The comparison of these distributions was based on the modified Kolmogorov–Smirnov goodness-of-fit test (Kececioglu, 1993). Fig. 10a and b illustrate the experimental CDF for Δ_{max} and Δ_{pl}, respectively, along with the theoretical CDFs for all considered distributions, for all three levels of KE_m considered.

In the modified Kolmogorov–Smirnov test, a proposed distribution is accepted at a given significance level, α, if the maximum difference between the experimental CDF and the theoretical CDF, D_n, is less than the critical value, $D_{n,\alpha}$, corresponding to the given level of significance (Ang and Tang, 1975). Based on the comparison between D_n and $D_{n,\alpha}$ values (calculated for the three statistical distributions at the three levels of KE_m) for significance levels $\alpha=5\%$ and $\alpha=1\%$, the truncated normal distribution is preferred over the normal and lognormal distribution (see Alphonso (2013)). These results are consistent with those from Herbin and Barbato (2012).

4.5. Effects of boundary conditions

The effects of different boundary conditions on the performance of aluminum storm panels were studied by conducting repeated impact tests at specified IP levels. In this test, two different installation options were considered: (1) a reference installation option without any support on the two long sides of the aluminum storm panel (shown in Fig. 6a and b), which corresponds to cases in which the panel is not wider than the opening to be protected; and (2) a new installation option in which the panel has some support on the two long sides of the aluminum storm panel (illustrated in Fig. 11), which corresponds to cases in which the panel is wider than the opening to be protected.

The new boundary conditions replicate the manufacturer-suggested mounting on a fixed rail system with a panel that overlaps the installation wall by 1.27 cm along the two unconstrained sides of the panels (i.e., the portions of the panel that are most vulnerable to penetrations). Installation of panels using these new boundary conditions assumes that (1) the wall is sufficiently strong to tolerate impact without damage (which is a reasonable hypothesis for brick and/or concrete walls), and (2) the distance between the panel and lateral support sides is sufficiently small to

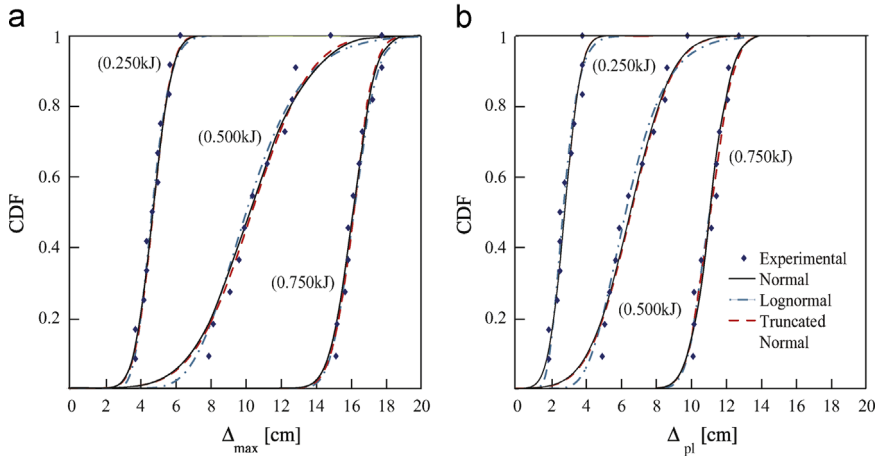

Fig. 10. CDFs relative to ordinary impacts for: (a) Δ_{max}, and (b) Δ_{pl}.

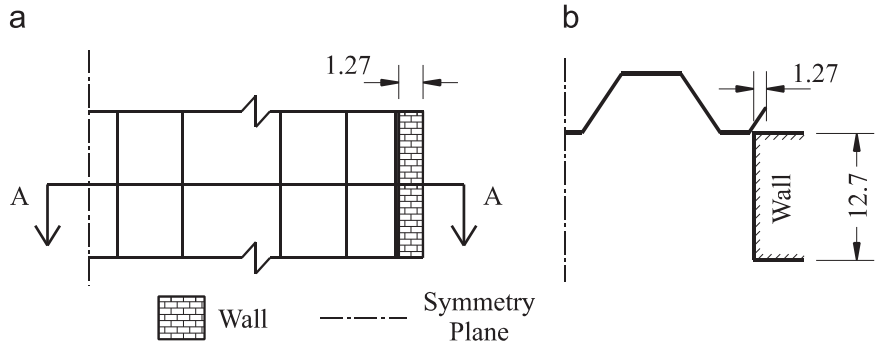

Fig. 11. New boundary condition case corresponding to an aluminum storm panel wider than the window opening: (a) elevation, and (b) section.

ensure contact between the panel and the sides under impact deformation. In order to represent this condition during testing, a steel plate was used to provide the support corresponding to the installation wall. It is noteworthy that both installation options are acceptable according to manufacturer's suggestions and code prescriptions, assuming that the distance between the panel and the side of the opening to be protected is smaller than ¼″ (6.35 mm).

This set of experimental test consisted of a total of 32 impact tests with random impact locations that were selected within the parabolic regions considered prone to penetration for each of the two installation options. In particular, 16 impact tests were conducted at $KE_m = 0.250$ kJ (actual variability: $0.238 \text{ kJ} \le KE_m \le 0.256$ kJ), and 16 impact tests were conducted at $KE_m = 0.500$ kJ (actual variability: $0.491 \text{ kJ} \le KE_m \le 0.520$ kJ) using a 9-lb missile. Figs. 12 and 13 show the impact locations and the corresponding impact types for $KE_m = 0.250$ kJ and $KE_m = 0.500$ kJ, respectively, as well as the parabolic regions vulnerable to penetration for (a) the reference boundary conditions, and (b) the new boundary conditions.

In the set of 16 impacts considering the reference boundary conditions, all impacts occurred within the two symmetric parabolic regions that are vulnerable to penetration. In this first set of tests, a total of 15 penetrations were recorded. Eight of these

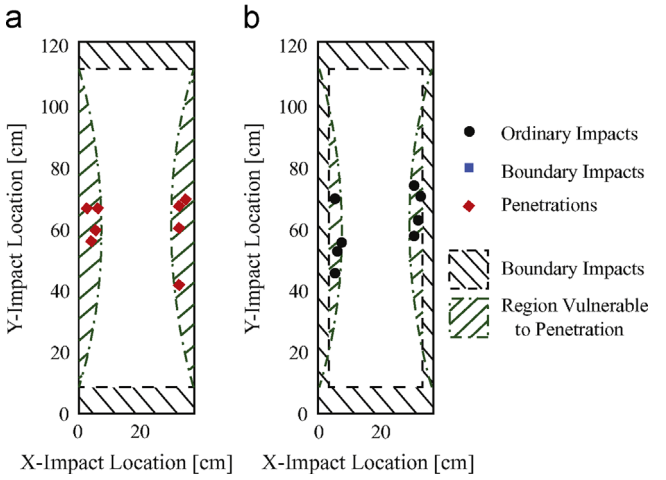

Fig. 12. Impact locations and corresponding impact types for $KE_m = 0.250$ kJ: (a) reference boundary conditions, and (b) new boundary conditions.

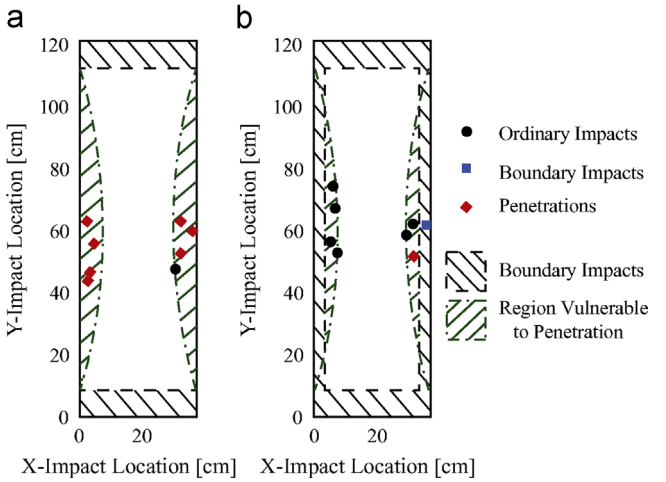

Fig. 13. Impact locations and corresponding impact types for $KE_m = 0.500$ kJ: (a) reference boundary conditions, and (b) new boundary conditions.

penetrations were recorded for $KE_m = 0.250$ kJ, corresponding to a probability of penetration conditional to impact occurring in the region vulnerable to impact (in short, conditional probability of penetration) equal to 100%. The other seven penetrations were recorded for $KE_m = 0.500$ kJ (corresponding to a conditional probability of penetration equal to 87.5%).

In the set of 16 impacts considering the new boundary conditions, 15 impacts occurred within the parabolic regions identified as vulnerable to penetration (one of which was the only actual penetration recorded), and one was a boundary impact on the boundary of the panel's long side, which was supported by the installation frame for the new boundary conditions. For this second set of tests, no penetration was recorded for $KE_m = 0.250$ kJ, and only one penetration was recorded for $KE_m = 0.500$ kJ, out of seven impacts occurring in the vulnerable region of the panel (corresponding to a conditional probability of penetration equal to 14.3%).

The large reduction in number of penetrations observed is very significant as it can be achieved via a small modification of the installation of the panel when protecting building envelope components. This installation modification could be easily implemented into practical installation applications by introducing it into building code's minimum requirements, i.e., by requiring a minimum value of overlap between walls and storm panels. With this modification, the region of the storm panel where boundary impacts take place becomes significantly larger than the region identified in the reference installation option. This new boundary region includes not only the boundary impact areas located at the top and bottom of the panel near the bolted connections with the fixed rail, but also two additional side regions along the unconstrained sides of the panel, which have a width equal to the width of the overlap between the wall and the storm panel plus one half of the missile width.

5. Damage analysis results and evaluation of fragility curves

The damage analysis phase of PBHE provides the probabilistic description of DMs or limit states for given values of EDPs. These results are then convoluted with the results of the structural analysis phase (i.e., the CDFs of the EDPs conditional to the value of KE_m, see Fig. 8a and b) to provide the desired fragility curves. This study considered the following three discrete limit states: (1) failure of the panel, (2) failure of the window behind the panel, and (3) complete penetration of the projectile. These three limit states are graphically illustrated in Fig. 14, where pictures of experimental results corresponding to failure for each of the three limit states considered are also provided in the insets.

Fig. 14a shows the limit state corresponding to failure of the panel only. In this scenario (i.e., panel failure), WBD impact causes the aluminum storm panel to reach an excessive plastic deformation, which renders the panel unusable in future hurricane events. This limit state failure is met when the value of Δ_{pl} is larger than or equal to a threshold ξ_{pl}, assumed to warrant replacement of the panel (i.e., $\Delta_{pl} \ge \xi_{pl}$). In this study, ξ_{pl} is assumed deterministically equal to 2.50 in (6.35 cm). Fig. 14b illustrates the limit state corresponding to excessive deformation of the panel resulting in the failure of both the panel and the window behind the panel. This limit state failure occurs when EDP Δ_{max} is larger than or equal to the threshold ξ_{max}, which is defined as the minimum distance between the aluminum storm panel and the window protected by the panel (i.e., $\Delta_{max} \ge \xi_{max}$). In this research, ξ_{max} is assumed deterministically equal to 5.00 in (12.70 cm). Fig. 14c illustrates the penetration of the panel and window after WBD impact. A test corresponding to a missile penetration is considered a failure also with respect to the other two limit states of interest.

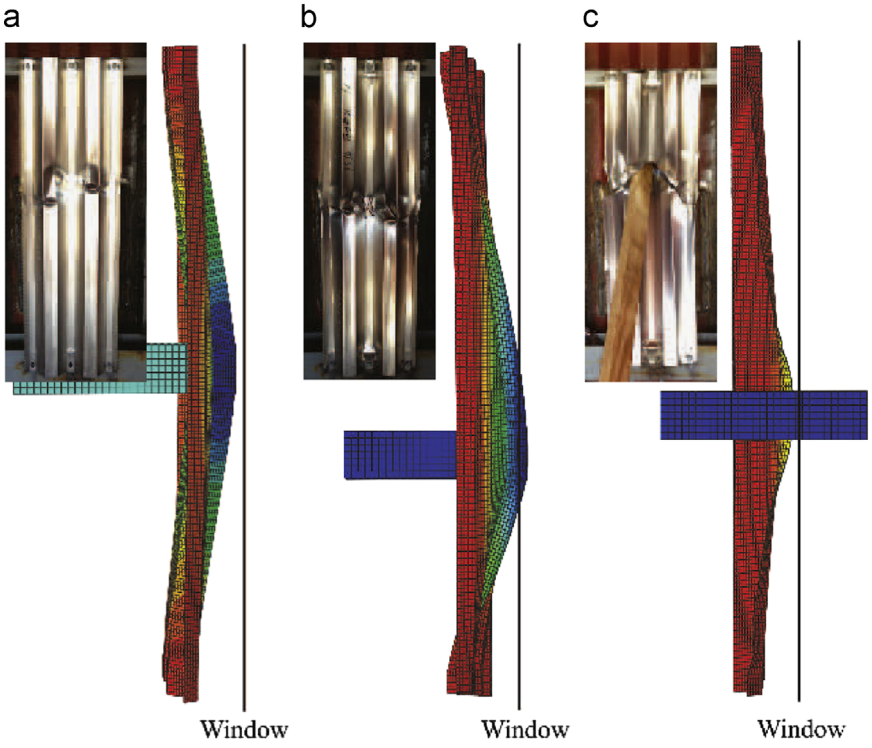

Fig. 14. Damage limit states: (a) failure of the storm panel, (b) failure of the window, and (c) penetration of the missile.

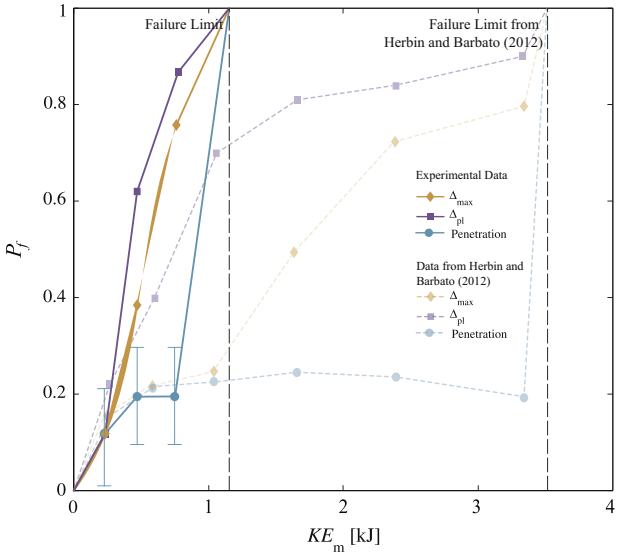

Fig. 15. Fragility curves for aluminum hurricane storm panels: comparison of experimental and numerical results.

The value of ξ_{max} adopted in this research represents a realistic value of the mean distance between panels and windows for common installations. However, for specific applications, appropriate statistics should be obtained from data regarding the specific window installation under study in the specific hurricane prone region of interest.

Fig. 15 compares the experimental fragility curves corresponding to the three limit states considered in this research with the numerical results found in Herbin and Barbato (2012). For the penetration limit state, the standard deviation of the failure probability estimator (which is a measure of the estimate's accuracy) is also provided. This standard deviation is relatively large when compared to the failure probability estimates for the penetration limit state, due to the relatively small number of penetrations recorded in the experimental tests.

A significant quantitative difference is observed between experimental and numerical fragility curves. In particular, when compared to the experimental results, the numerical fragility curves derived in Herbin and Barbato (2012) are slightly higher for $KE_m = 0.250$ kJ, whereas they provide lower probability of failure values for all limit states at higher values of KE_m. In addition, the experimental and numerical failure limits (i.e., the values of KE_m corresponding to almost certain physical failure of the aluminum panels and identified in Fig. 15 by vertical dashed lines) are equal to 1.15 kJ and 3.50 kJ, respectively. These discrepancies are most likely due to the fact that the modeling assumptions for the boundary conditions made in Herbin and Barbato (2012) did not correspond to the behavior that was observed experimentally for the bolted connections between the storm panel and the support frame. The reference boundary conditions considered in this study consisted of three bolted connections with ¾″ bolts at the top and bottom sides of the panel, as recommended by the installation instructions provided by the manufacturer (AGI Group, personal communication) and consistent with the requirements of the 2010 Florida Building Code (ICC, 2011). In Herbin and Barbato (2012), these connections were modeled using fixed boundary conditions, i.e., by assuming that the portion of the panels surrounding the bolted connection was rigidly connected to the supporting frame. However, the experimental tests showed that, for $KE_m \geq 1.150$ kJ, the panels began tearing at the bolted connections, splitting the aluminum below the bolt and separating the panel from the target support frame (Fig. 7a). This type of failure is inconsistent with the modeling assumptions adopted in Herbin and Barbato (2012). As a consequence of these inaccurate modeling assumptions for the boundary conditions, the stiffness and strength of the aluminum panels were significantly overestimated in Herbin and Barbato (2012).

6. Additional considerations on applicability and scope of this research

The results presented in this paper indicate that the current standard for impact protective systems' performance (i.e., ASTM E1866 and E1996, ASTM, 2005a, 2005b) are inconsistent with modern performance-based design approaches. In fact, these standard are based on simplistic pass/no pass criteria and, for metal storm panels, do not distinguish among different failure limit states and do not provide information on the fragility curves, which are an essential ingredient of PBHE. This paper presents an approach for developing fragility curves of windborne debris impact protective systems. This approach involves: (1) defining pertinent limit states; (2) identifying appropriate IPs; and (3) performing experimental tests to derive the fragility curves. The first two steps should be based on existing and future research on different typologies of windborne debris protection systems (e.g., systems with brittle or ductile behavior). The third step should be regulated in future standards and should be tailored to the different types of protection systems, materials, installation conditions, and types of missiles.

It is noteworthy that, while the methodology proposed in this paper to derive fragility curves for windborne debris impact protective systems is general, the specific experimental results and their interpretation are valid only for the specific conditions considered in this experimental campaign, i.e., for a single aluminum panel with direct mount through bolted connections impacted by wooden 2×4 missiles. Additional experimental investigations are needed to study the effects of (1) overlapping multiple panels (which is the most common installation condition in real-world applications); (2) different mount options (e.g., track mount versus direct mount); (3) different materials (e.g., steel versus aluminum); and (4) different missiles (e.g., roof tiles versus wooden 2×4 missiles).

7. Conclusions

The research presented in this paper focused on the derivation of experimental fragility curves for windborne debris (WBD) impact risk assessment of building envelope components with ductile behavior (in particular, aluminum storm panels) within a recently developed performance-based hurricane engineering (PBHE) framework. In PBHE, fragility curves represent the cumulative distribution functions (CDFs) of damage measures or discrete limit states, expressed in terms of appropriate interaction parameters (IPs) that are used to describe the intensity of the WBD impact.

Three limit states were identified in this research: (1) damage to the storm panel (with engineering demand parameter defined as the maximum plastic deformation of the panel, Δ_{pl}); (2) damage to the window protected by the storm panel (with engineering demand parameter defined as the maximum total deflection of the panel, Δ_{max}); and (3) complete penetration of the panel by the projectile.

A first set of experimental tests was performed to identify a sufficient IP for the three limit states considered in this study. It was found that the impact kinetic energy, KE_m, is a sufficient IP for aluminum storm panels impacted by 2×4 wooden missiles. It is suggested that KE_m may be a sufficient IP also for other building envelope components with ductile behavior, and that this hypothesis should be verified through additional experimental testing.

A second set of experimental tests was performed to derive experimental fragility curves for the three considered limit states. Three typologies of impacts were identified: (1) ordinary impacts; (2) boundary impacts (i.e., impacts occurring in the area of the panels that is connected to the support frame, whose effects are mainly dependent on the installation details of the storm panel and on the strength of the supporting wall); and (3) complete panel penetrations. It was also found that the location of impact on the panel plays a large role in determining the impact type and level of damage to the structure. Experimental CDFs for both Δ_{max} and Δ_{pl} were developed and used to derive analytical CDFs for ordinary impacts.

A third set of experimental tests was performed to evaluate the effects of installation details (i.e., boundary conditions) on the performance of aluminum storm panels. It was found that a small overlap between the storm panel and the supporting wall along the panel's free sides decreases significantly the vulnerability of the panel to penetration. These results suggest that the addition of a minimum overlap requirement in the building code's specifications for storm panels could have a very beneficial effect on the safety of structures subjected to WBD impact hazard; whereas it may require only a minimal change in common application practices and it may cause an insignificant cost increase for the building's owners.

Acknowledgments

The authors gratefully acknowledge partial support of this research by the Louisiana Board of Regents (LA BoR) through the Pilot Funding for New Research (Pfund) Program of the National Science Foundation (NSF) Experimental Program to Stimulate Competitive Research (EPSCoR) under Award no. LEQSF(2013)–PFUND-305, and the Longwell's Family Foundation through the Fund for Innovation in Engineering Research (FIER) Program. Any opinions, findings, conclusions or recommendations expressed in this publication are those of the authors and do not necessarily reflect the views of the sponsors.

References

Alphonso, T.C., 2013. (Master's thesis). Experimental Fragility Analysis of Aluminum Storm Panels Subject to Windborne Debris. Department of Civil and Environmental Engineering, Louisiana State University and A&M College, Baton Rouge, LA, USA.

Ang, A.H.S., Tang, W.H., 1975. Probability Concepts in Engineering Planning and Design, Vol. 1. John Wiley & Sons, Inc., New York, NY, USA.

American Society for Testing and Materials (ASTM) International, 2005a. Standard specification for performance of exterior windows, curtain walls, doors and impact protective systems impacted by windborne debris in hurricanes. ASTM Standard E1996. West Conshohocken, PA, USA.

American Society for Testing and Materials (ASTM) International, 2005b. Standard test method for performance of exterior windows, curtain walls, doors, and impact protective systems impacted by missile(s) and exposed to cyclic pressure differentials. ASTM Standard E1886. West Conshohocken, PA, USA.

Applied Technology Council (ATC), 1997. NEHRP Guidelines for the Seismic Rehabilitation of Buildings, FEMA 273.

Applied Technology Council (ATC), 2005. Development of next-generation performance-based seismic design procedures for new and existing buildings. ATC-58. Redwood City, CA, USA.

Augusti, G., Ciampoli, M., 2006. First steps towards performance-based wind engineering, Performance of Wind Exposed Structures: Results of the PERBACCO Project. Firenze University Press, Florence, Italy.

Autodesk Inc., 2013. Autodesk REVIT Structures version 2013. Computer Software, San Rafeal, CA, USA.

Barbato, M., Petrini, F., Unnikrishnan, V., Ciampoli, M., 2013. Probabilistic performance-based hurricane engineering (PBHE) framework. Struct. Saf. 45, 24–35.

Baker, J.W., Cornell, C.A., 2005. A vector-valued ground motion intensity measure consisting of spectral acceleration and epsilon. Earthq. Eng. Struct. Dyn. 34 (10), 1193–1217.

Baker, J.W., Cornell, C.A., 2008. Vector valued intensity measures incorporating spectral shape for prediction of structural response. J. Earthq. Eng. 12 (4), 534–554.

Borges, A., Lopez R.R., Godoy L.A., Lopez, R.E.Z., 2009. Impact of windborne debris on storm shutters. In: Proceedings of the 11th Americas Conference on Wind Engineering, San Juan, PR, USA, June 22–26.

Ciampoli, M., Petrini, F., Augusti, G., 2011. Performance-based wind engineering: towards a general procedure. Struct. Saf. 33, 367–378.
Cornell, C.A., Krawinkler, H., 2000. Progress and challenges in seismic performance assessment. PEER Cent. News 3 (2), 1–4.
Fernandez, G., Masters, F.J., Gurley, K.R., 2010. Performance of hurricane shutters under impact by roof tiles. Eng. Struct. 32 (1), 3384–3393.
Gardoni, P., Der Kiureghian, A., Mosalam, K.M., 2002. Probabilistic Models and Fragility Estimates for Bridge Components and Systems (Report PEER-2002/13, PEER Center). University of California, Berkeley, CA, USA.
Gurley, K., Pinelli, J.P., Subramanian, C., Cope, A., Zhang, L., Murphree, J., Artiles, A., Misra, P., Gulati, S., Simiu, E., 2005. Florida Public Hurricane Loss Projection Model Engineering Team Final Report Volume II: Predicting the Vulnerability of Typical Residential Buildings to Hurricane Damage (Technical report, International Hurricane Research Center). Florida International University, Miami, FL, USA.
Hamburger, R.O., Whittaker A.S., 2003. Considerations in performance-based blast resistant design of steel structures. In: Proceedings of the AISC-SINY Symposium on Resisting Blast and Progressive Collapse, American Institute of Steel Construction, New York, NY, USA, December 4-5.
Holmes, J., 2008. Windborne debris and damage risk models: a review. In: Proceedings of the Advances in Wind and Structures Conference, Jeju, Korea, May 29–31.
Holmes, J., 2010, Rational wind-load design and wind-load factors for loactions affected by tropical cyclones, hurricanes, and typhoons. In: Proceedings of the Structures Congress 2010, Orlando, Fl, USA, May 12–15.
Herbin, A., Barbato, M., 2012. Fragility curves for building envelope components subject to windborne debris impact. J. Wind Eng. Ind. Aerodyn. 107–108 (1), 285–298.
International Code Council (ICC), 2011. 2010 Florida Building Code. International Code Council, Inc., Washington, DC, USA.
Kececioglu, D., 1993. Reliability and Life Testing Handbook, Vol. 1. Prentice Hall, Englewood Cliffs, NJ, USA.
Kentang, L., 2000. An analysis of the recent severe storm surge disaster events in China. Nat. Hazards 21 (2), 215–223.
Kwon, O., Kim, E., Orton, S., 2010. Calibration of the live load factor in LRFD bridge design specifications based on state-specific traffic environments. J. Bridge Eng. 16 (6), 812–819.
Laboy, S., Smith, D., Gurley, K.R., Masters, F.J., 2013. Roof tile frangibility and puncture of metal window shutters. Wind Struct. 17 (2), 185–202.
Li, Y., Ellingwood, B., 2006. Hurricane damage to residential construction in the US: importance of uncertainty modeling in risk assessment. Eng. Struct. 28 (7), 1009–1018.
Lin, N., Vanmarcke, E., 2010. Windborne debris risk analysis—Part I. Introduction and methodology. Wind Struct. 13 (2), 191–206.
Lin, N., Vanmarcke, E., Yau, S.-C., 2010. Windborne debris risk analysis—Part II. Application to structural vulnerability modeling. Wind Struct. 13 (2), 207–222.
Lopez, C., Masters, F.J., Bolton, S., 2011. Water penetration resistance of residential window and wall systems subjected to steady and unsteady wind loading. Build. Environ. 46 (7), 1329–1342.
Luco, N., Cornell, C.A., 2007. Structure-specific scalar intensity measures for near-source and ordinary earthquake ground motions. Earthq. Spectra 23 (2), 357–392.
Lupoi, G., Franchin, P., Lupoi, A., Pinto, P., 2006. Seismic fragility analysis of structural systems. J. Eng. Mech. 132 (4), 385–395.
Mackie K., Stojadinovic B., 2004. Fragility curves for reinforced concrete highway overpass bridges. In: Proceedings of the 13th World Conference on Earthquake Engineering, Vancouver, Canada, August 1–6.
Masters, F.J., Gurley, K.R., Shah, N., Fernandez, G., 2010. The vulnerability of residential window glass to lightweight windborne debris. Eng. Struct. 32 (4), 911–921.
McDonald, J., 1990. Impact resistance of common building materials to tornado missiles. J. Wind Eng. Ind. Aerodyn. 36 (1–3), 717–723.
Minor, J., Harris, P., Beason, W., 1978. Designing for windborne missiles in urban areas. J. Struct. Division 104 (11), 1749–1760.
National Association of Home Builders (NAHB) Research Center, 2002. Wind-borne debris impact resistance of residential glazing. U.S. Department of Housing and Urban Development, Office of Policy Development and Research, Cooperative Agreement H-21172CA, Washington, DC, USA.
National Science Board (NSB), 2007. Hurricane Warning: The Critical Need for a National Hurricane Research Initiative. NSB-06-115. National Science Foundation, Arlington, VA, USA.
Nowak, A.S., 1999. (Calibration of LRFD Bridge Design Code). Transportation Research Board, Washington, DC, USA (Report 368).
Pielke, R.A., Gratz, J., Landsea, C.W., Collins, D., Saunders, M.A., Musulin, R., 2008. Normalized hurricane damage in the United States: 1900–2005. Nat. Hazards Rev. 9 (1), 29–42.
Pinelli, J.-P., Simiu, E., Gurley, K., Subramanian, C., Zhang, L., Cope, A.D., Filliben, J., Hamid, S., 2004. Hurricane damage prediction model for residential structures. J. Struct. Eng. 130 (11), 1685–1691.
Porter, K., 2003. An overview of PEER's performance-based earthquake engineering methodology. In; Proceedings of the Conference on Applications of Statistics and Probability in Civil Engineering, San Francisco, CA, USA, July 6–9.
Rini, D., Lamont, S. 2008. Performance based structural fire engineering for modern building design. In: Proceedings of the Structures Congress 2008: Crossing Borders, pp. 1–12.
Shooting Chrony, 2014. User's Manual for Shooting Chrony®s Chronographs, Models: Beta and Gamma Shooting Chrony®s and Beta and Gamma Master Chrony®s. Shooting Chrony, Inc., Amherst, NY, USA ⟨http://www.shootingchrony.com/manual_BG.htm⟩ (accessed on March 2014).
Stewart, M.J., 2003. Cyclone damage and temporal changes to building vulnerability and economic risks for residential construction. J. Wind Eng. Ind. Aerodyn. 91 (5), 671–691.
Tachikawa, M., 1983. Trajectories of flat plates in uniform flow with application to wind-generated missiles. J. Wind Eng. Ind. Aerodyn. 14 (1–3), 443–453.
Tachikawa, M., 1988. A method for estimating the distribution range of trajectories of wind-borne missiles. J. Wind Eng. Ind. Aerodyn. 29 (1–3), 175–184.
Twisdale, L.A., Vickery, P.J., Steckley, A.C., 1996. Analysis of Hurricane Windborne Debris Impact Risk for Residential Structures (Report 5303). Applied Research Associates, Raleigh, NC, USA.
Vamvatsikos, D., Cornell, C.A., 2005. Developing efficient scalar and vector intensity measures for IDA capacity estimation by incorporating elastic spectral shape information. Earthq. Eng. Struct. Dyn. 34 (13), 1573–1600.
Willis, J.A.B., Lee, B.E., Wyatt, T.A., 2002. A model of windborne debris damage. J. Wind Eng. Ind. Aerodyn. 90 (4–5), 555–565.